LONG-TERM DISPERSION MODELLING: ASSESSMENT OF ATMOSPHERIC TRANSPORT AND DEPOSITION PATTERNS FROM NUCLEAR RISK SITES IN EURO-ARCTIC REGION

A. Mahura

Danish Meteorological Institute, Copenhagen, Denmark
Institute of the Northern Environmental Problems,
Kola Science Center, Apatity, Russia
Ecole Centrale de Nantes, France
e-mail: mahura@dmi.dk

A. Baklanov, J. H. Sørensen
Danish Meteorological Institute, Copenhagen, Denmark
e-mail: ???

Описывается проверка разработанной методологии оценки ядерных рисков, уязвимости и вероятности долговременного атмосферного переноса и осаждения радиоактивных загрязнений из 16 выбранных потенциальных источников ядерного загрязнения в регионы Европейской Арктики. Идентифицированы географические территории и прилегающие к ним страны, подвергающиеся наибольшему загрязнению в случае гипотетической аварии в зоне риска.

Introduction

Many international research projects have realized models and methods describing separate parts in evaluation of risk assessment, e. g. probabilistic safety assessment, long-range transport and contamination modelling, radioecological sensitivity, dose estimation, etc. However, methodologies for multidisciplinary studies of nuclear risk assessments and mapping are not well developed yet (cf. e. g. [3]). As shown by [1, 2], the risk-assessment strategy can be realised by the following methods: inference from actual events (i. e. using published results from real events), physical modelling (i. e. using known input and prevalent levels), and theoretical modelling (i. e. using simulated response to assumed scenarios of releases). Description and results of these methods with respect to nuclear risk sites are shown by [4–10].

For probabilistic analysis certain studies are based on combination of different factors and probabilities. Previous research for the Arctic latitudes were based on trajectory modelling approach to evaluate potential impacts from nuclear plants such as Kola [11, 12] and Bilibino

METEOROLOGICAL DATA ARCHIVES

| NCAR | ECMWF | DMI-HIRLAM | Other archives |

Data Extracting and Pre-processing

TRAJECTORY AND DISPERSION MODELLING

| Isentropic Trajectory Model | DMI-Trajectory Model | DERMA-Model of Long-Range Transport | Models of Local Scale | Other Models |

STATISTICAL ANALYSIS OF MODELLING RESULTS

| Exploratory Data Analysis of Trajectories | Cluster Analysis of Trajectories | Probability Fields Analysis | Other Methods of Statistical Analysis |

CHARACTERISTICS AND INDICATORS OF NRS IMPACT

Simple Characteristics for Selected Geographical Regions:
- Upper & Lower Boundaries of NRS Impact
- Average Transport Time
- Atmospheric Transport by Layers
- Fast Transport, etc.

Atmospheric Transport Pathways

Maximum Reaching Distance and Maximum Possible Impact Zone

Probability Fields

| Airflow | Precipitation and Relative Humidity | Fast Transport |
| Mixing Layer Height | Dry, Wet and Total Deposition | Concentration and Doses |

Typical Transport Time Field

Other Characteristics and Indicators

GIS COMPLEX RISK ASSESSMENT

Pre-processing and Using of DataBases

| Nuclear Risk Objects | Population and risk groups | Administrative Boundaries | Radioecological Sensitivity of Territories |
| Economical Factors | Social Factors | Other Factors | Political Factors |

GIS Modelling of NRS Impact

Fig. 1. Scheme of the probabilistic risk analysis based on dispersion and trajectory modelling approaches.

[13]. The dispersion modelling approach was used by Slaper [14] who evaluated dispersion of the radioactive plume by a simple model (based on only one meteorological station) in order to estimate risks, health effects, and countermeasures due to severe accidents at European nuclear plants (including the northern latitudes plants) and a submarine [15]. Sinyak [16] used empirical factors to describe the influences of geography resulting in normalized damage factors for the main European cities. Andreev [17, 18] simulated dispersion and deposition with a Lagrangian particle model and calculated the frequency of exceedance of certain thresholds for ^{137}Cs regarded as a risk indicator.

The dispersion and deposition models can be successfully used for separate case studies for likely or worst-case scenarios. They can be used also for probabilistic risk mapping as a more expensive, but alternative of the trajectory analysis methods discussed by [19, 20]. Applicability and examples of different dispersion and deposition models on the local and regional scales for accidental releases in the Arctic were discussed by [21–25].

The methodology, developed in the bounds of the "Arctic Risk" NARP project [1] is a logical continuation of previous studies. It includes several specific approaches in optimal strategy of multidisciplinary methodology. Among these approaches is a combination of probabilistic and case study analyses. The suggested scheme for multidisciplinary risk assessment, which includes a combination of trajectory and dispersion modelling and statistical analysis, is shown in fig. 1. For assessment of risk and vulnerability different indicators are considered, including the social-geophysical factors, which depend on the location and population of the area of interest and probabilities, as well as approaches and modelling tools. As shown in fig. 1, there is a variety of research tools in the methodology scheme of probabilistic risk and vulnerability assessments. In this paper the suggested multidisciplinary approach and illustration of dispersion modelling tool involved are described. Note that, for example, other approaches also include modelling and clustering of trajectories [13, 26], specific case studies [12], and evaluation of vulnerability and consequences to radioactive deposition [27, 28].

The main purpose of this paper is to test and employ the developed methodology (e.g. [1, 2]) based on long-term dispersion modelling in order to evaluate temporal and spatial variability of atmospheric transport and deposition patterns from 16 nuclear risk sites (NRSs) in the Euro-Arctic region, and use these patterns for further integration in GIS for risk and vulnerability mapping.

1. Selected approaches

1.1. Nuclear risk sites of interest

The selected NRSs are located within the area of interest of the "Arctic Risk" NARP Project. These sites are represented mostly by nuclear power plants (NPPs) in Russia, Lithuania, Germany, United Kingdom, Finland, Ukraine, and Sweden (see fig. 2). The Kola NPP (KNP, Murmansk Region, Russia) has the VVER-230 type of reactors; Leningrad (LNP, Leningrad Region, Russia), Chernobyl (CNP, Ukraine), and Ignalina (INP, Lithuania) NPPs have the RBMK-type reactor of major concern. Moreover, the Novaya Zemlya (NZS, Novaya Zemlya Archipelago, Russia) was considered as a former nuclear weapon test range and potential site for nuclear waste deposit; and the Roslyakovo shipyard (KNS, Murmansk Region, Russia) was considered as a risk site with nuclear power ships in operation or waiting to be decommissioned.
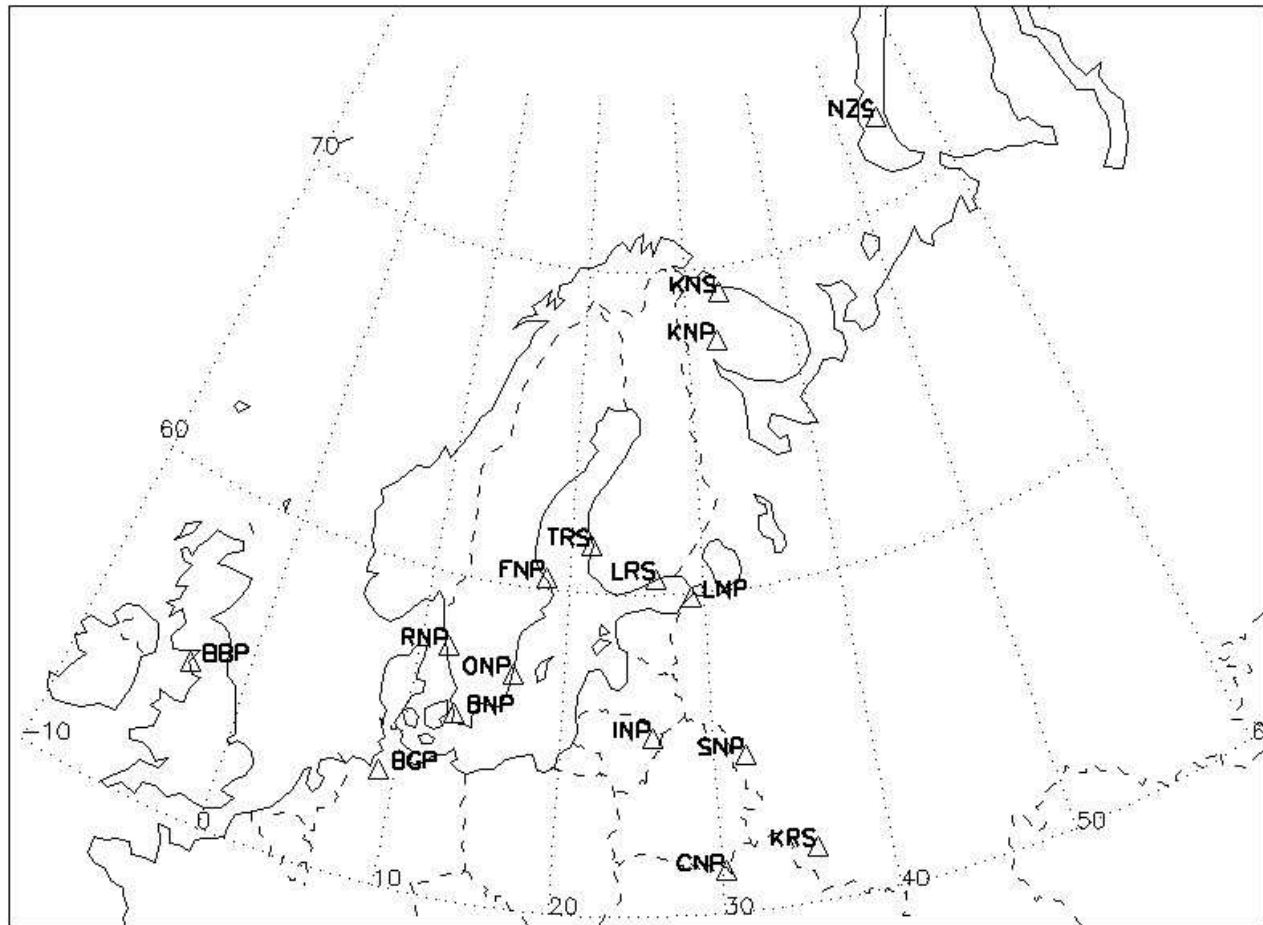
Fig. 2. Selected nuclear risk sites (KNP — Kola nuclear power plant (NPP); LNP — Leningrad NPP; NZS — Novaya Zemlya test site; INP — Ignalina NPP; BBP — block of British NPPs; BGP — block of German NPPs; LRS — Loviisa NPP; TRS — Olkiluoto NPP; ONP — Oskarshamn NPP; RNP — Ringhals NPP; BNP — Barsebaeck NPP; FNP — Forshmark NPP; KRS — Kursk NPP; SNP — Smolensk NPP; CNP — Chernobyl NPP; KNS — Roslyakovo shipyard).

The BBP site is represented by a group of British risk sites: the Sellafield reprocessing plant and closely located NPPs in this area. The BGP site is represented by a group of German NPPs, which are closely located too. Although these plants use different reactor types and, hence, could have different risks of accidental releases, the grouping is relevant for airborne transport studies because NPPs are located geographically close to each other and, hence, individual atmospheric transport patterns will be relatively similar. Further evaluation of risk levels can be calculated for each plant separately based on the atmospheric transport fields and probabilities of accidents for each plant.

1.2. Input meteorological data

In our study, two types of gridded datasets — from the Danish Meteorological Institute (DMI) — HIgh Resolution Limited Area Model (HIRLAM) and the European Centre for Medium-Range Weather Forecast (ECMWF) — were used as input data. Detailed description of datasets is given by [2].

The DMI-HIRLAM dataset was used to model atmospheric transport, dispersion, and deposition of ^{137}Cs for 16 NRSs during Fall 2001 – Fall 2003. The ECMWF dataset (domain covers nearly the entire Northern Hemisphere, i.e. extends between 12°N–90°N and 180°W–180°E) was used to model atmospheric transport, dispersion, and deposition for three radionuclides — ^{137}Cs, ^{131}I, and ^{90}Sr — but only from one NRS (Leningrad NPP, Russia).

1.3. Long-term dispersion modelling using DERMA

The Danish Emergency Response Model for Atmosphere (DERMA), developed by DMI for nuclear emergency preparedness purposes, is a numerical 3-D atmospheric model of Lagrangian type. DERMA was used to simulate long-term (2001–2003) atmospheric transport, dispersion, and deposition of radionuclide from the selected NRSs. It consideres also processes of radioactive decay, dry and wet removal by precipitation during atmospheric transport. As input meteorological data, DERMA uses: Numerical Weather Prediction (NWP) model data from different operational versions of DMI-HIRLAM, or ECMWF global model data. Detailed description of the DERMA model and assumptions used in this study are given by [2].

The following variables (for a daily continuous discrete unit hypothetical release (DUHR) of ^{137}Cs at risk sites at rate of 10^{11} Bq/s) were calculated: 1) air concentration (Bq/m^3) in the surface layer; 2) time integrated air concentration, TIAC (Bq·h/m^3); 3) dry deposition, DD (Bq/m^2), and 4) wet deposition, WD (Bq/m^2) fields. Then, these fields were interpolated into a gridded domain (30–89°N and 60°W–135°E) with a resolution of 0.5° latitude vs. 0.5° longitude. Moreover, these fields were limited by 5 days of atmospheric transport of radioactive matter after release ended at risk sites.

The SGI Origin scalar server was used for DERMA runs and the NEC SX6 supercomputer system of DMI was used for DMI-HIRLAM modelling computational purposes.

1.4. Probabilistic analysis for dispersion modelling results

The dispersion modelling results can be analysed in a similar manner as for trajectory modelling [19, 20]. Two approaches were considered to construct probability fields for the TIAC, DD, and WD patterns. In both approaches for calculation of fields, only data with "valid dates" were used (i.e. when original meteorological data were available for computation).

The first approach (based on the results of dispersion modelling) considers the distribution of the total sum of daily continuous DUHR of radioactivity at the site during the time period of interest (month, season, or year). LetTs call this field the summary field, because it is integrated over a considered period. This type of field shows the most probable geographical distribution of the radionuclide TIAC (DD, WD) at the surface if the release of radioactivity occurred during the period of interest. The second approach is simply based on calculating the average value from the summary field obtained in the first approach. LetTs call this field the average field. This type of field shows the average distribution of the radionuclide TIAC (DD, WD) at the surface when the release of radioactivity occurred during one average day within the period of interest.

Note, for convenience of comparison the temporal variability (between months or seasons) of patterns can be underlined by isolines at similar intervals, although every field could be reconstructed with different threshold orders of magnitude than those selected.

2. Assessment of long-term atmospheric dispersion from nuclear risk sites in Euro-Arctic region

The focus is evaluation of long-term dispersion, which is represented as potential indicators of the NRS impact. Only the average fields are discussed, although the summary fields are also available [20]. The scaling with similar magnitude isolines starting from the lowest of 10^{+2} (1e+2 in figures) is used to simplify interpretation and comparison of fields, although other scales can be selected and fields re-plotted based on the original archived data. Additionally, the estimation of the TIAC, DD, WD, and total deposition (TD) patterns resulted from atmospheric accidental releases at NRS was performed for selected European cities.

Note that, first, using the average and summary fields it is possible to interpolate data to a particular geographical area of interest (enclosed by geographical boundaries) or for a particular geographical location (for example, a city). Second, the summary fields can be used to calculate doses accumulated over a period (month, season, or year) — i. e. monthly doses, seasonal doses, or annual doses. These summary fields will be more representative for the routine discharges of radioactivity from NRS. Third, the average fields will be used further to calculate doses accumulated from a one day hypothetical release averaging over a considered period — i. e. average daily doses for a particular period. These average fields will be more representative for the accidental short-term releases of radioactivity from NRS. Fourth, the summary fields will have larger areas enclosed by isolines, and magnitudes of concentration and deposition will be higher compared with the average fields. Fifth, because all fields were calculated for the discrete unit hypothetical release, it is possible to recalculate or rescale these fields for other accidental releases of radioactivity at different magnitude rates. Sixth, in simulation of atmospheric transport and deposition of daily radioactivity releases from NRS, our calculations were limited to 5 days after the release was completed at the site. As uncertainties in modelling of atmospheric transport after 5 days became too great, for the calculated fields of one-day releases we did not apply any loss processes after that 5 day term. It might be that after this term the trajectories still did not leave the model grid domain and following the mass conservation law these trajectories will provide additional contributions into concentration and deposition fields. But, we assume, that mostl trajectories will leave the selected domain with regions of interest in our study and contributions at boundaries of the calculated fields will be significantly smaller. Moreover, once radionuclide was deposited on the surface, the radioactive decay was not considered, although it should be accounted for further risk and vulnerability assessment.

Note that in this study the probabilities and severities of possible accidents from different types of nuclear risk sites are not considered, and only geophysical factors of atmospheric transport and deposition are taken into account.

2.1. Annual average time integrated air concentration patterns of ^{137}C

The time integrated air concentration (TIAC) of a radionuclide is used as input to calculate doses accumulated due to inhalation. Some common peculiarities should be mentioned. First, the TIAC fields have a distribution around the site, which is, in general, closer to elliptical than circular. Second, the shape of these fields, reflects the presence of dominating airflow patterns throughout the year. Similar patterns were also obtained from the results of the trajectory modelling, cluster analysis, and airflow probability fields analysis of 5-day trajectories given

by [20]. Third, the largest values of TIAC were observed near the sites, and they decreased significantly with distance, as expected.

The annual average TIAC fields for selected risk sites are shown in fig. 3 (the seasonal and monthly variabilities of the average and summary TIAC fields for the rest of the sites are given by [20]). On an annual scale, the highest TIAC ($\geq$1e+3 Bq·h/m^3) are within the first few hundred kilometres around all NRSs. The isolines of 1e+2 Bq·h/m^3 for both Arctic sites — NZS and KNS — are more extended in the southern sector from the sites compared to the northern sector. For the NZS site, this isoline passes over unpopulated areas compared with the KNS and KNP sites. The populated territories of the Kola Peninsula and Karelia as well as northern territories of Norway and Finland are enclosed by the same isoline, and these remained more affected by potential accidental releases compared with other territories. Note, when only atmospheric trajectories for the NZS site were used to construct the airflow probability fields (see analysis of trajectory modelling results by [20]) than the total area of the territories situated under the potential impact from this site was higher compared with other sites. The dispersion approach, however, gave another picture because of including effects of stronger dispersion for the strong wind situations in the Arctic latitudes.
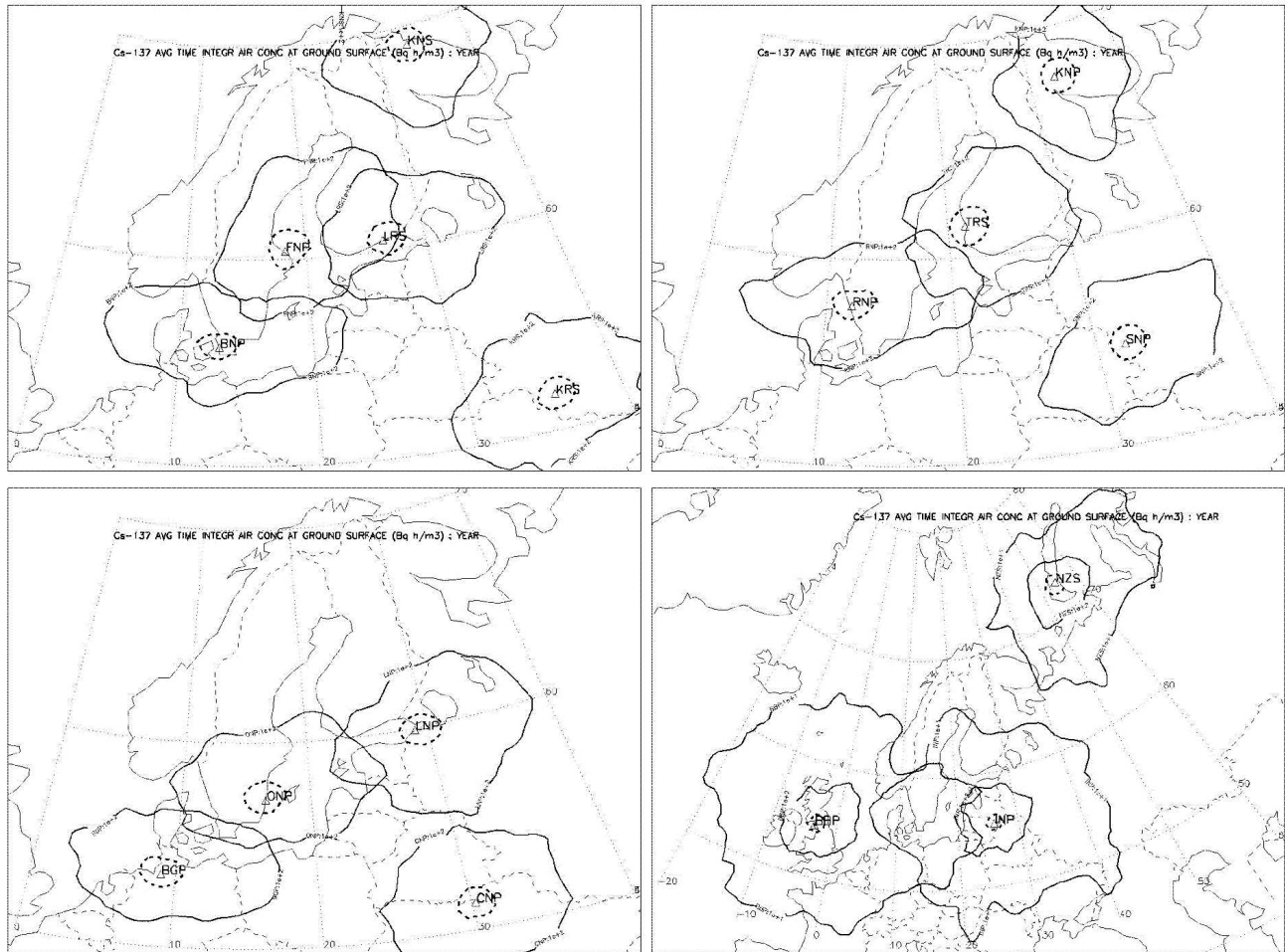
Fig. 3. Annual average time integrated air concentration fields for the selected nuclear risk sites in the Euro-Arctic region. Izolines are drawn starting from "NRS:1e+1" Bq h/m^3.

Annual average ^{137}Cs time integrated air concentration (TIAC), dry (DD), wet (WD), and total depositions (TD), and relative contribution of dry (DD/TD) and wet (WD/TD) depositions into total deposition at selected European cities resulted from hypothetical release at the Leningrad nuclear power plant

City, Country	Dist to LNP, km	TIAC, Bq·h/m^3	DD, Bq/m^2	WD, Bq/m^2	TD, Bq/m^2	DD/TD, %	WD/TD, %
St.Petersburg, Russia	70	2.75E+3	1.48E+4	3.45E+4	4.93E+4	30	70
Tallinn, Estonia	245	1.80E+2	9.70E+2	1.14E+3	2.11E+3	46	54
Helsinki, Finland	424	5.28E+1	2.85E+2	7.51E+2	1.04E+3	28	72
Riga, Latvia	435	6.36E+1	3.43E+2	3.11E+2	6.54E+2	52	48
Stockholm, Sweden	618	3.48E+1	1.88E+2	1.60E+2	3.48E+2	54	46
Vilnius, Lithuania	622	4.31E+1	2.33E+2	1.52E+2	3.85E+2	61	39
Minsk, Belarus	673	3.73E+1	2.01E+2	1.81E+2	3.83E+2	53	47
Moscow, Russia	686	4.07E+1	2.20E+2	4.75E+2	6.94E+2	32	68
Warszawa, Poland	983	8.01E+0	4.32E+1	2.38E+1	6.71E+1	64	36
Oslo, Norway	1014	8.28E+0	4.47E+1	1.60E+2	2.04E+2	22	78
Kiev, Ukraine	1057	6.85E+0	3.70E+1	7.23E+1	1.09E+2	34	66
Copenhagen, Denmark	1077	1.50E+1	8.10E+1	7.68E+1	1.58E+2	51	49
Berlin, Germany	1261	7.99E+0	4.31E+1	5.21E+1	9.53E+1	45	55
Praha, Czech Republic	1426	3.13E+0	1.69E+1	2.75E+1	4.44E+1	38	62
Bratislava, Slovakia	1515	1.70E+0	9.16E+0	1.37E+1	2.29E+1	40	60
Budapest, Hungary	1522	1.32E+0	7.10E+0	4.26E+0	1.14E+1	62	38
Vienna, Austria	1535	1.42E+0	7.66E+0	1.43E+1	2.19E+1	35	65
Amsterdam, Netherlands	1699	3.15E+0	1.70E+1	6.56E+0	2.36E+1	72	28
Bucharest, Romania	1731	1.39E+0	7.53E+0	4.07E+0	1.16E+1	65	35
Brussels, Belgium	1840	3.09E+0	1.67E+1	6.77E+0	2.35E+1	71	29
Luxembourg, Luxembourg	1845	1.91E+0	1.03E+1	4.08E+0	1.44E+1	72	28
Torshavn, Faeroes	1920	2.89E-1	1.56E+0	1.39E+0	2.96E+0	61	39
Bern, Switzerland	2012	3.75E-1	2.03E+0	1.19E+1	1.39E+1	15	85
London, UK	2025	2.12E+0	1.14E+1	9.14E+0	2.06E+1	56	44
Paris, France	2095	1.50E+0	8.07E+0	3.20E+0	1.13E+1	72	28
Dublin, Ireland	2246	1.25E-1	6.73E-1	2.00E+0	2.67E+0	25	75
Reykjavik, Iceland	2625	1.19E-1	6.43E-1	5.95E-1	1.24E+0	52	48
Nuuk, Greenland	3939	9.58E-6	5.17E-5	3.89E-5	9.06E-5	53	47

The structure of the concentration field for the BBP site reflects the fact that the most impacted territories are the British Islands. The potentially affected areas for other sites, except the Kursk and Chernobyl NPPs, are extended within the 50–65°N latitudinal belt. For NRSs of the Scandinavian countries, the affected territories are domestic areas of the Nordic countries, Baltic States, and border areas of the Northwest Russia. The ^{137}Cs concentrations were estimated at the most populated European cities using as an example the annual average TIAC field from the Leningrad NPP (tabl. 1). At these cities the TIAC decreases by two orders of magnitude within the first 500 km range from the plant. The highest TIAC — 2.75e+3 Bq·h/m3 — is at St.Petersburg, Russia due to proximity to the nuclear plant. Within the next 500 km range the TIAC values varied between the zero and first orders of magnitude, after that TIAC decreased by an additional order of magnitude reaching a minimum of 3.75e–1 Bq·h/m^3 at Bern, Switzerland. After 2000 km of atmospheric transport from the LNP site the initial TIAC decreased mostly by three-four orders of magnitude compared with the area closer to the plant. The concentration at the far city (Nuuk, Greenland) was even by 9 orders of magnitude smaller — 9.58e–6 Bq·h/m^3.

2.2. Annual average dry and wet deposition patterns of ^{137}C

The dry (DD) and wet (WD) depositions of a radionuclide are input data to calculate doses from the underlying surface and further to the nutrition pathways. Similar to TIAC, for example, the annual average DD and WD fields can be used to calculate the average dose from the underlying surface at any selected geographical location at any given day of the year.

The DD patterns reflect the structure of the TIAC patterns. Therefore, the elliptical configurations of both fields are similar. The DD reaches its highest values in vicinity of the site. Dry deposition fields are as a reliable indicator of the prevailing atmospheric transport patterns as an airflow probability field. In particular, for all selected NRSs there is a clear tendency of atmospheric transport by westerly flows. The WD patterns are different from the TIAC and DD patterns. The WD fields are less smooth and often have a cellular structure, because they reflect the irregularity of the rainfall patterns.

The annual average DD and WD fields for several NRSs are shown in fig. 4 (the seasonal and monthly variabilities of the average and summary DD and WD fields for the rest of the sites are given by [20]). The highest DDs are in vicinity of the sites (fig. 4, top). Taking into account isolines of similar magnitude, note that the DD fields are more extended in the N–S (3–6 degrees) and W–E (5–10 degrees) directions compared with the TIAC fields (fig. 3). For example, considering an isoline of 1e+2 Bq/m^2, for the Arctic NRSs, the affected populated areas are extended more to the south and west of the sites covering large parts of the Northwest Russia and Finland. For the NZS site, it is extended more in the western and eastern directions reaching the Kanin and Yamal Peninsulas, respectively. For the British site, these boundaries passed further to the north and east of the site compared with the same order of magnitude isoline of the TIAC field. For the European sites, these boundaries reached as far south as 50°N. For the Scandinavian NPPs, the isolines reached as far north as the Kola Peninsula with a significant extension in the eastern direction too. For the KRS, CNP, and SNP plants, these boundaries almost reached the Black Sea aquatoria.

The highest WD (1e+4 Bq/m^2) is seen within a 300–400 km range of the sites (fig. 4, bottom). The WD fields are more extended in all directions compared with both TIAC and DD fields. For example, considering an isoline of 1e+2 Bq/m^2, for the Arctic sites the affected populated areas are extended farther to the south and west of the sites covering the northern parts of Norway, Sweden, most of Finland, and Northwest Russia (south of 60°N). For the NZS site, it is extended even farther to the east (east of 70°E) of the site, and reached the Kola Peninsula territories. For the British site, the WD field boundaries extended farther in the NW–NE sector reaching populated Iceland at north and the Scandinavian and inland European countries at east. For the European risk sites, these boundaries reached south of 50°N and east of 40°E. For the Scandinavian NPPs, these boundaries reached as far north as the Barents Sea with a significant extension in the eastern direction passing through the 50°E longitude. For the KRS, CNP, and SNP plants, the WD boundaries passed over the Black Sea aquatoria and almost reached the Caspian Sea.

As shown in tabl. 1, on example of a hypothetical release from the Leningrad NPP, the contribution of the wet deposition compared with the dry deposition into the total deposition varied significantly from city to city. Among the considered capitals, 8 showed approximately equal contribution of both depositions — 50±5 %. The WD contribution is more than 65 % of TD for another 8 cities selected in this study. The DD contribution is more than 65 % of TD for another 5 cities including the Benelux countries, Romania, and France, and which are located farther west from the LNP site.
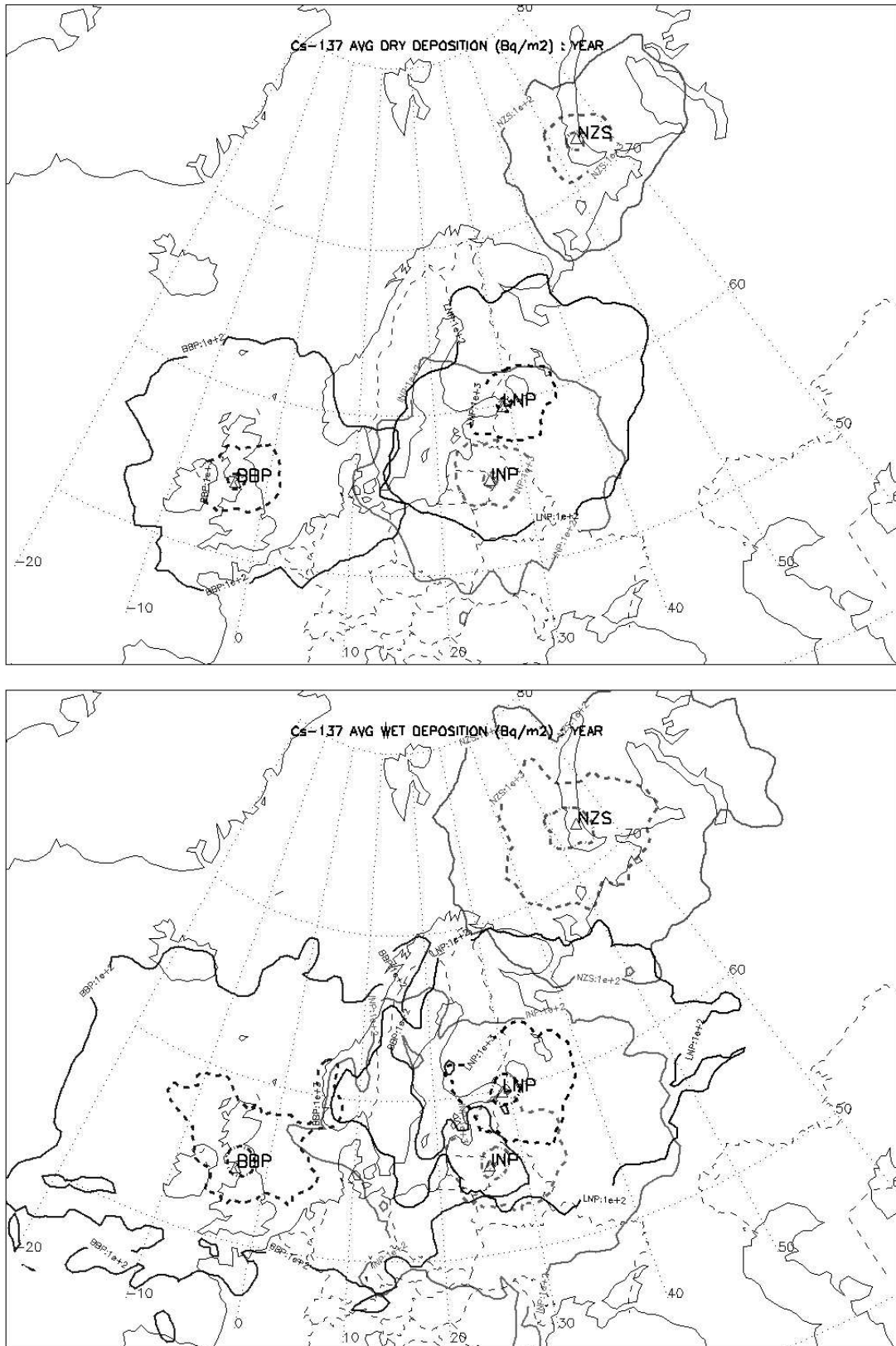
Fig. 4. Annual average dry deposition (top) and wet deposition (bottom) fields for the British plants (BBP), Ignalina plant (INP), Leningrad plant (LNP), and Novaya Zemlya test site (NZS). Izolines are drawn starting from "NRS:1e+2" Bq/m2).

2.3. General statistics, correlations between patterns, and seasonal variability

The concentration of different pollutants may differ by orders of magnitude, and in statistical analyses the use of log-transformation on original data is considered as a useful step. In our study, all calculated ^{137}Cs TIAC, DD, and WD fields were initially log-transformed, and then subsequent set of descriptive statistics (on example of the Leningrad NPP) — including range, variance, standard deviation, minimum and maximum, and mean, skewness and kurtosis with a standard error — was calculated (tabl. 2). The calculated distribution histograms of log-transformed data for all fields have the skewed (in the section of the lower values — to the left) nature. As seen from the table, all characteristics are higher for WD compared with two other fields.

The correlations were estimated between the TIAC, DD, and WD fields. The best fit of data was presented by a linear regression. All fields showed a statistically significant (applying the 2-tailed test) strong positive correlation (with $R^2 \approx$ 0.972–0.999), with a correlation of TIAC vs. DD higher compared with both TIAC vs. WD and DD vs. WD correlations.

The concentration and depositions were evaluated as a function of radial distance from the Leningrad NPP as shown in fig. 5. These were also evaluated using a box-plot procedure with a grouping into several classes by distance from the site. The highest concentrations and depositions are generally occurred within the first 1000 km range from the LNP site with a low variability of 1–2 orders of magnitude. After 1000 km, the range of their variability became larger — within several (6–10) orders of magnitude, although the mean decreased normally following the radioactive decay. The gap between 3000–5000 km reflects differences in the airflow patterns from this site. In particular, the higher concentrations were more often observed to the south of the site (i. e. south of LNP latitude — 59.9°N) than to the north of the site, but beyond 4000 km they became comparable. Similarly, it is higher for the east (i. e. west of LNP longitude — 29°E) compared with the west. It is mportant to note that the focus of this study is on the regional scale of the Northern Europe, and therefore, our region of interest is limited up to 4000 km from the site.

On a seasonal scale (figs 6, 7, top), the highest magnitude TIAC isolines (1e+3 Bq·h/m^3) are concentrated around the sites and mostly they have a circle-oriented shape; although for the British site, during summer it is significantly extended in the eastern direction and during winter — in the north-western direction of the site (fig. 7, top-left). For the Ignalina site (fig. 6, top-left), during summer it is more extended in the western direction, and during winter — in the eastern direction. The highest concentrations are more characteristic for the border regions of Lithuania, Latvia, and Belarus. For the NZS site, during all seasons it is more concentrated in the NW-SW sector of the site, and it is extended almost twice farther to the west compared

Table 2

Descriptive statistics for the log-transformed annual average 137Cs time integrated air concentration (TIAC), dry (DD), and wet (WD) deposition fields for the Leningrad nuclear power plant

Log-Transformed Field	Range	Min	Max	Mean	Std. Dev	Variance	Skewness	Kurtosis
TIAC	12.60	−6.00	6.60	0.88±0.01	2.33	5.41	−0.45±0.01	−0.34±0.03
DD	13.34	−6.00	7.34	1.57±0.01	2.38	5.65	−0.53±0.01	−0.12±0.03
WD	13.67	−6.00	7.67	1.79±0.01	2.39	5.71	−0.59±0.01	−0.03±0.03
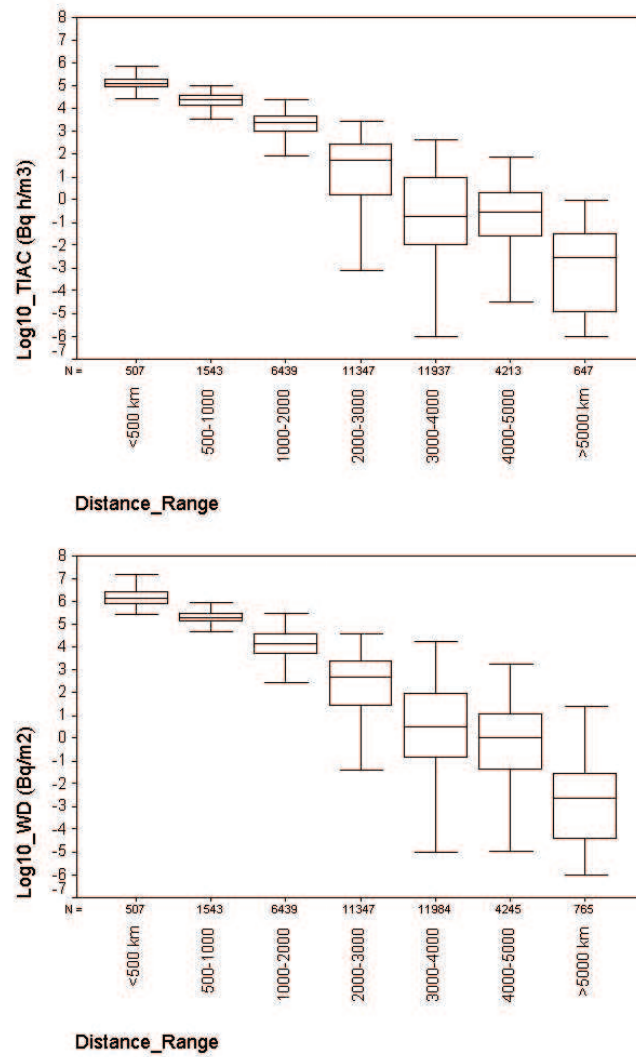
Fig. 5. Annual average time integrated air concentration (top) and wet deposition (bottom) fields (on a logarithmic scale) as a function of radial distance range from the Leningrad nuclear power plant.

with the east (fig. 7, top-right).

Similarly, the TIAC isolines of $1e+2$ Bq·h/m^3 are more extended in the directions of main airflow from the sites and they have more an elliptical than a circlar shape. For the BBP site (fig. 7, top-left) during atmospheric transport such concentrations were not even observed at the seashore of the European continent. These TIACs occurred mostly over the British Islands and adjacent seas. For the INP site (fig. 6, top-left), during summer the same isoline is more extended (almost twice) in the western direction than during winter — in opposite, eastern direction of the site. During spring, the extension is more pronounced along the NE-SW section. Among the Scandinavian countries, the TIAC can reach magnitudes of $1e+2$ Bq·h/m^3 at the Baltic seashore counties of Sweden only during summer, and south of Finland — only during spring. For the NZS site (fig. 7, top-right), during winter a significant extension in the NW direction from the site is occurred, and during summer the area of the TIAC field is almost twice larger compared with other seasons. Throughout the year the populated Russian territories were practically unaffected by these concentrations. Moreover, the seasonal variability of the NZS TIAC field varied within a 5-degree latitudinal belt.

    The further analyses of the seasonal DD and WD fields for the same risk sites (figs 6, 7,
middle & bottom) showed more complex structures, and especially for WD. The DD fields
are significantly extended (especially during summer in the southern directions) from the sites
compared with the TIAC fields. The WD fields showed multiple cells. This reflected a cellular
structure of precipitation patterns. These WD fields are also farther extended from the sites
compared with the DD fields.
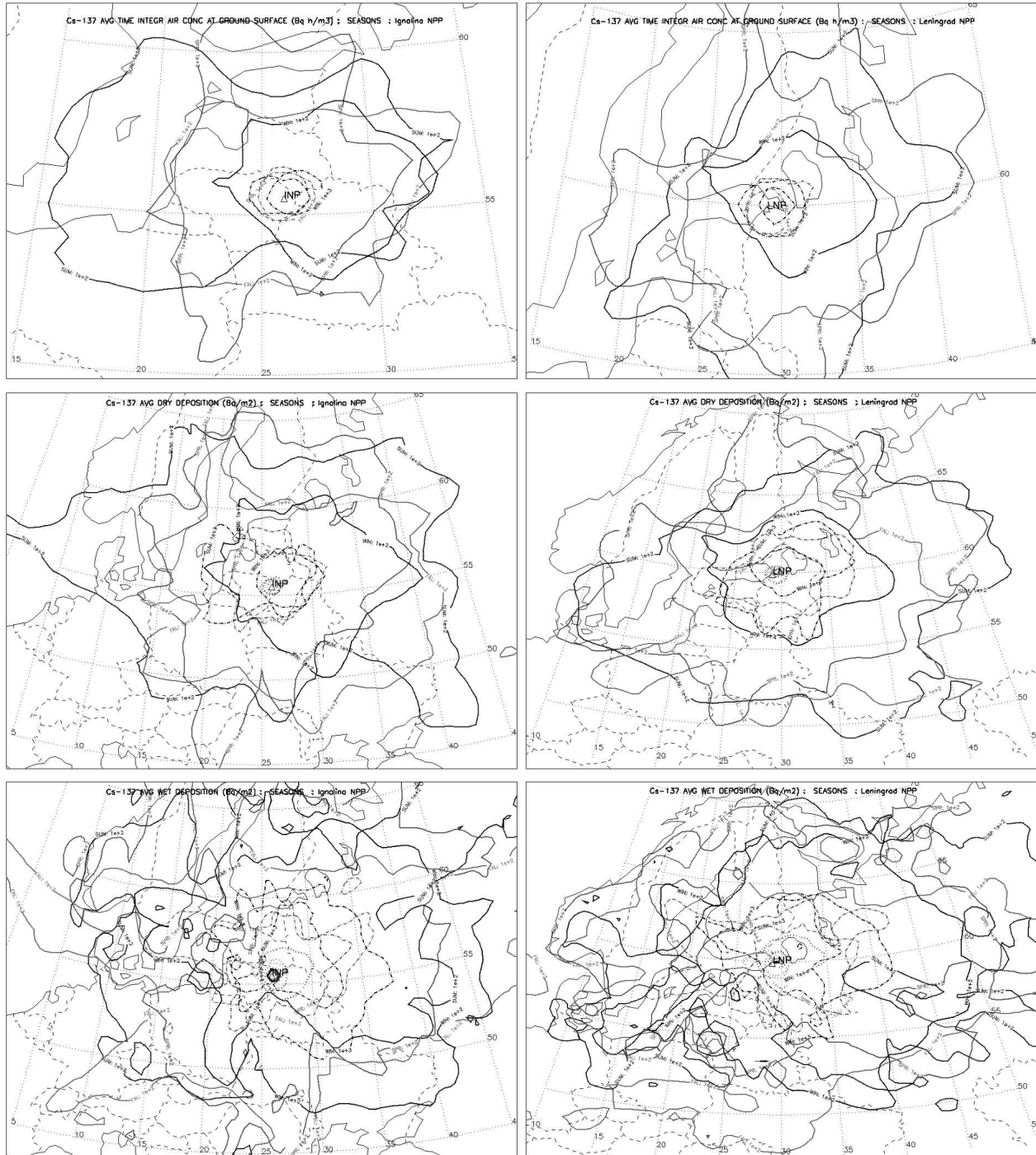
Fig. 6. Seasonal average time integrated air concentration (top), dry deposition (middle) and wet
deposition (bottom) fields for the Ignalina plant, INP (left) and Leningrad plant, LNP (right).

In particular, the multiple-cell structure of WD is well seen during all seasons for the British site (fig. 7, bottom-left) compared with the Ignalina and Novaya Zemlya sites. This multiplicity depends strongly on peculiarities of the maritime climate of the BBP site. Wet depositions as high as 1e+3 Bq/m^2 are observed during winter-summer in the western part of Norway, during winter — in Denmark, during fall — in Iceland and western seashore territories of Germany
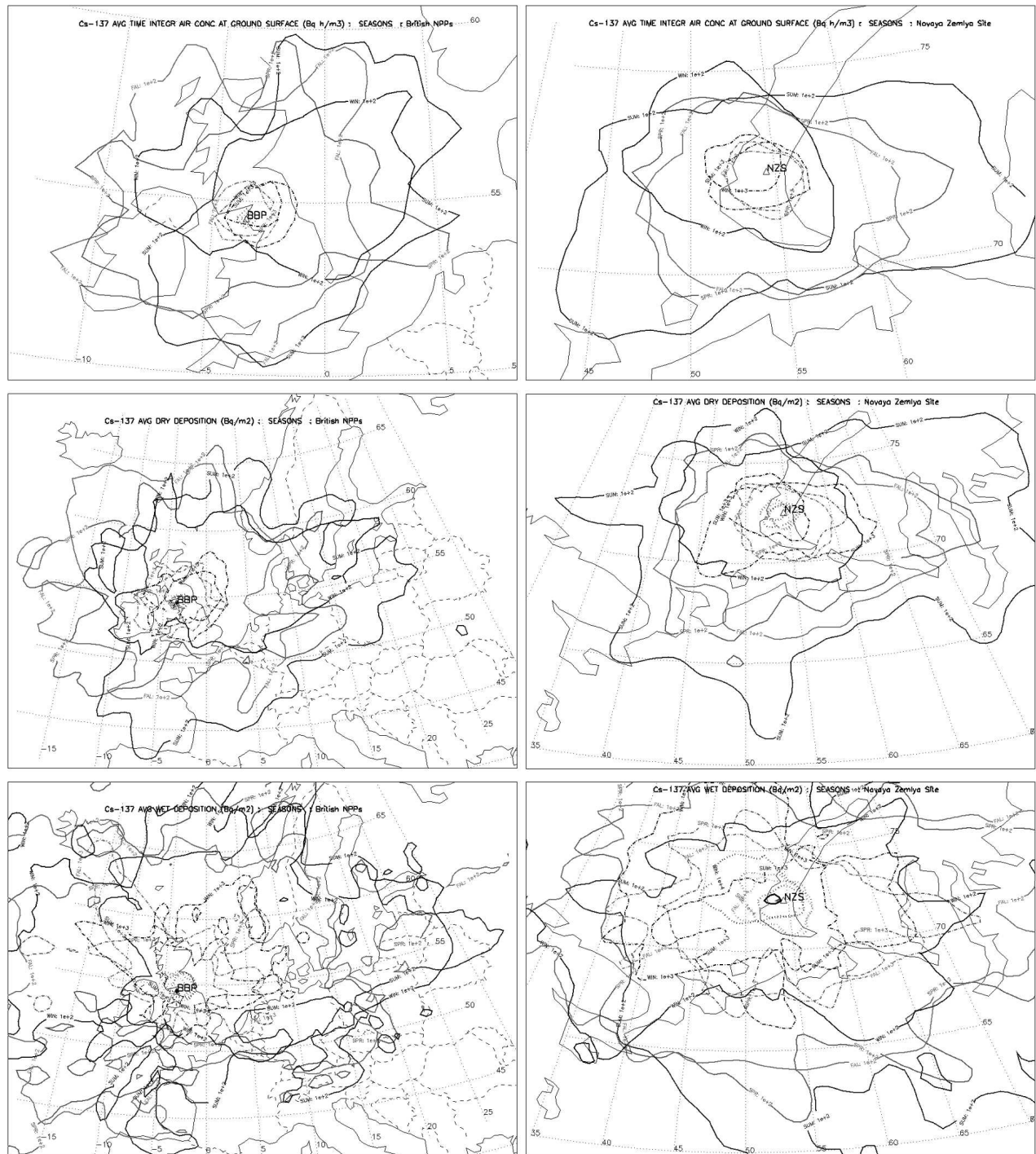
Fig. 7. Seasonal average time integrated air concentration (top), dry deposition (middle) and wet deposition (bottom) fields for the British plants, BBP (left) and Novaya Zemlya test site, NZS (right).

and Benelux countries. The areas of wet depositions of 1e+2 Bq/m² are extended to the south passing at 45°N and to the east passing at 30°E.

The multiple-cell structure of WD is less pronounced for the Ignalina NPP (fig. 6, bottom-left). This site is more attributed to the inland, and hence, it is related to a more continental type of the climate. During summer, although DD is higher in the E–S sector, WD is more characteristic for the territories situated north of the site. During winter, the areas enclosed by isolines of 1e+3 Bq/m² are almost 2.5 times larger for WD compared with DD field, and these are more extended in the eastern directions from the site. Hence, throughout the year the dry deposition of 1e+3 Bq/m² is observed mostly over the Baltic States and northern Belarus. The wet deposition of the same order of magnitude is characteristic for a wider area, especially during winter, covering additionally territories of the Northwest Russia, Belarus, Ukraine, and Poland, as well as extending farther into the Baltic Sea aquatoria. Cells of the local maxima for WD are more often observed to the west of the site compared with the eastern directions (i. e. farther to the Eurasian continent).

T a b l e 3

Seasonal variability of average 137Cs wet deposition patterns at selected European cities resulted from hypothetical release at the Leningrad nuclear power plant

City, Country	Dist to LNP, km	Spr	Sum	Fal	Win	Ann	Max	Min	Max vs. Ann
St.Petersburg, Russia	70	2.89E+4	1.68E+4	1.20E+4	8.03E+4	3.45E+4	Win	Fal	2.3
Tallinn, Estonia	245	1.36E+2	6.37E+2	2.47E+3	1.30E+3	1.14E+3	Fal	Spr	2.2
Helsinki, Finland	424	6.02E+1	5.71E+2	1.89E+3	4.78E+2	7.51E+2	Fal	Spr	2.5
Riga, Latvia	435	4.62E+2	1.68E+1	4.56E+2	3.09E+2	3.11E+2	Spr	Sum	1.4
Stockholm, Sweden	618	1.14E+2	1.19E+2	3.73E+2	3.32E+1	1.60E+2	Fal	Win	2.3
Vilnius, Lithuania	622	1.14E+2	1.20E+2	2.36E+2	1.37E+2	1.52E+2	Fal	Spr	1.6
Minsk, Belarus	673	2.79E+2	8.46E+1	2.30E+2	1.32E+2	1.81E+2	Spr	Sum	1.5
Moscow, Russia	686	8.32E+2	1.21E+2	5.80E+2	3.65E+2	4.75E+2	Spr	Sum	1.8
Warszawa, Poland	983	1.33E+1	5.23E+1	2.91E+1	6.32E-1	2.38E+1	Sum	Win	2.2
Oslo, Norway	1014	2.54E+2	2.43E+2	1.31E+2	1.06E+1	1.60E+2	Spr	Win	1.6
Kiev, Ukraine	1057	1.04E+1	1.26E+1	2.20E+2	4.58E+1	7.23E+1	Fal	Spr	2.9
Copenhagen, Denmark	1077	2.43E+1	1.59E+2	1.23E+2	2.12E-1	7.68E+1	Sum	Win	2.1
Berlin, Germany	1261	1.87E+1	1.21E+2	6.56E+1	3.04E+0	5.21E+1	Sum	Win	2.3
Praha, Czech Republic	1426	9.94E-1	5.79E+1	5.11E+1	2.62E-2	2.75E+1	Sum	Win	2.1
Bratislava, Slovakia	1515	2.38E+0	1.15E+1	4.09E+1	3.84E-3	1.37E+1	Fal	Win	3.0
Budapest, Hungary	1522	1.58E+0	1.19E+0	1.42E+1	5.52E-2	4.26E+0	Fal	Win	3.3
Vienna, Austria	1535	1.34E+0	1.49E+0	5.43E+1	2.29E-4	1.43E+1	Fal	Win	3.8
Amsterdam, Netherlands	1699	5.53E+0	1.30E+1	7.72E+0	1.66E-6	6.56E+0	Sum	Win	2.0
Bucharest, Romania	1731	4.21E+0	4.97E-1	1.07E+1	8.29E-1	4.07E+0	Fal	Win	2.6
Brussels, Belgium	1840	1.33E+1	1.12E+1	2.64E+0	1.62E-6	6.77E+0	Spr	Win	2.0
Luxembourg, Luxembourg	1845	1.91E+0	5.55E+0	8.85E+0	2.31E-5	4.08E+0	Fal	Win	2.2
Bern, Switzerland	2012	2.47E-1	1.78E+0	4.55E+1	6.78E-8	1.19E+1	Fal	Win	3.8
London, UK	2025	1.24E+1	4.52E+0	1.97E+1	3.34E-7	9.14E+0	Fal	Win	2.2
Paris, France	2095	1.15E+1	7.27E-1	5.52E-1	5.38E-5	3.20E+0	Spr	Win	3.6
Dublin, Ireland	2246	5.36E-2	2.03E-1	7.73E+0	2.05E-4	2.00E+0	Fal	Win	3.9
Reykjavik, Iceland	2625	1.42E+0	6.10E-1	3.53E-1	9.87E-4	5.95E-1	Spr	Win	2.4

For the Artic latitude site — Novaya Zemlya Archipelago (fig. 7, bottom-right) — the WD pattern showed less variability in precipitation patterns. The WD field has no well-underlined patterns of irregularity compared with other discussed sites. Throughout the year, depositions of more than 1e+3 Bq/m^2 are not observed over populated Russian territories. During summer, dry deposition of a lesser order of magnitude (1e+2 Bq/m^2) can be observed over the Murmansk and Archangelsk Regions. The WD of the same magnitudes for the same regions is characteristic during all seasons, although during winter-fall the areas enclosed by these isolines are extended farther to the Scandinavian Peninsula, and during spring-summer they are more extended to the south (down to 60°N).

The evaluation of seasonal variability of the ^{137}Cs WD patterns at selected cities (tabl. 3) showed that WD could be as much as 3.9 times higher during a particular season compared with the annual WD. This is a characteristic situation in Dublin, Ireland during fall. Among selected cities the lowest rate of maximum vs. annual WD is 1.4 (Riga, Latvia). Moreover, the rate of more than 3 is observed for cities located farther than a 1500 km circle from the Leningrad plant. The minimum WDs are more characteristic during winter. It was observed at 17 among 26 cities selected, and all these cities are located farther than 900 km from the site. The difference between the annual and minimum varied up to 8 orders of magnitude at that time, although this difference was only up to 1 order of magnitude when a minimum was observed during other seasons.

2.4. Specific case studies for ^{137}C, ^{131}I, AND ^{90}SR releases

The specific case studies approach, compared with the long-term dispersion modelling, have some peculiarities and criteria for selection discussed by [2]. This approach is computationally less expensive, but it allows estimating further risk and vulnerability only on particular dates. Alternatively, it provides a possibility to evaluate potential consequences of an accident for worst-case meteorological situations. Some case studies with evaluation of possible consequences were considered for the Kola nuclear power plant [12] and nuclear submarine bases of the Russian Northern and Pacific Fleets [2, 6, 20, 28].

In our study, the selected specific case is date of 24th August 2000. For this case, the atmospheric transport, dispersion, and deposition were evaluated for ^{137}Cs, ^{131}I, and ^{90}Sr (as major dose-contributing radionuclides) considering DUHR (at a fixed rate of 10^{11} Bq/s) occurred during 24 hours (24–25 August 2000, 00 UTC) at the Leningrad NPP. As input meteorological data the ECMWF model output was used. The total amount of radioactivity released during a one-day release was equal to 8.64·10^{15} Bq. For simplification this amount was the same for all radionuclides. Different release heights are not considered because such sensitivity studies were carried out by [6, 24]. Note, the simulation results can be easily recalculated for any scenario of accident

For this specific date, during the first two days, atmospheric transport generally occurred in the eastern direction from the LNP site. During the 3rd day, the contaminated cloud continued transport by westerlies, although motion to the west also became pronounced. During the 4th day, the directions of the separated cloud transport did not change significantly, except that the southern component became evident. During the 5th and 6th days, one part of the cloud, which initially moved to the east, propagated to the south passing over aquatoria of the Black Sea and Ukraine. The other part of the cloud, which previously moved to the west, continued to the north passing over the Scandinavian countries. Comparison of ^{137}Cs/^{90}Sr and ^{131}I (long-lived vs. short-lived) radionuclides reflected a significant decrease of concentration during atmospheric

transport. This especially is seen on the last days (fig. 8; note, due to similarities for ^{137}Cs and ^{90}Sr fields, the latter is omitted). Only small areas over the Scandinavian Peninsula and Black Sea were still affected by the presence of ^{131}I on the 6th day, although for ^{137}Cs, the affected area remained relatively large, extending between the south of the Scandinavian Peninsula and the Black Sea.
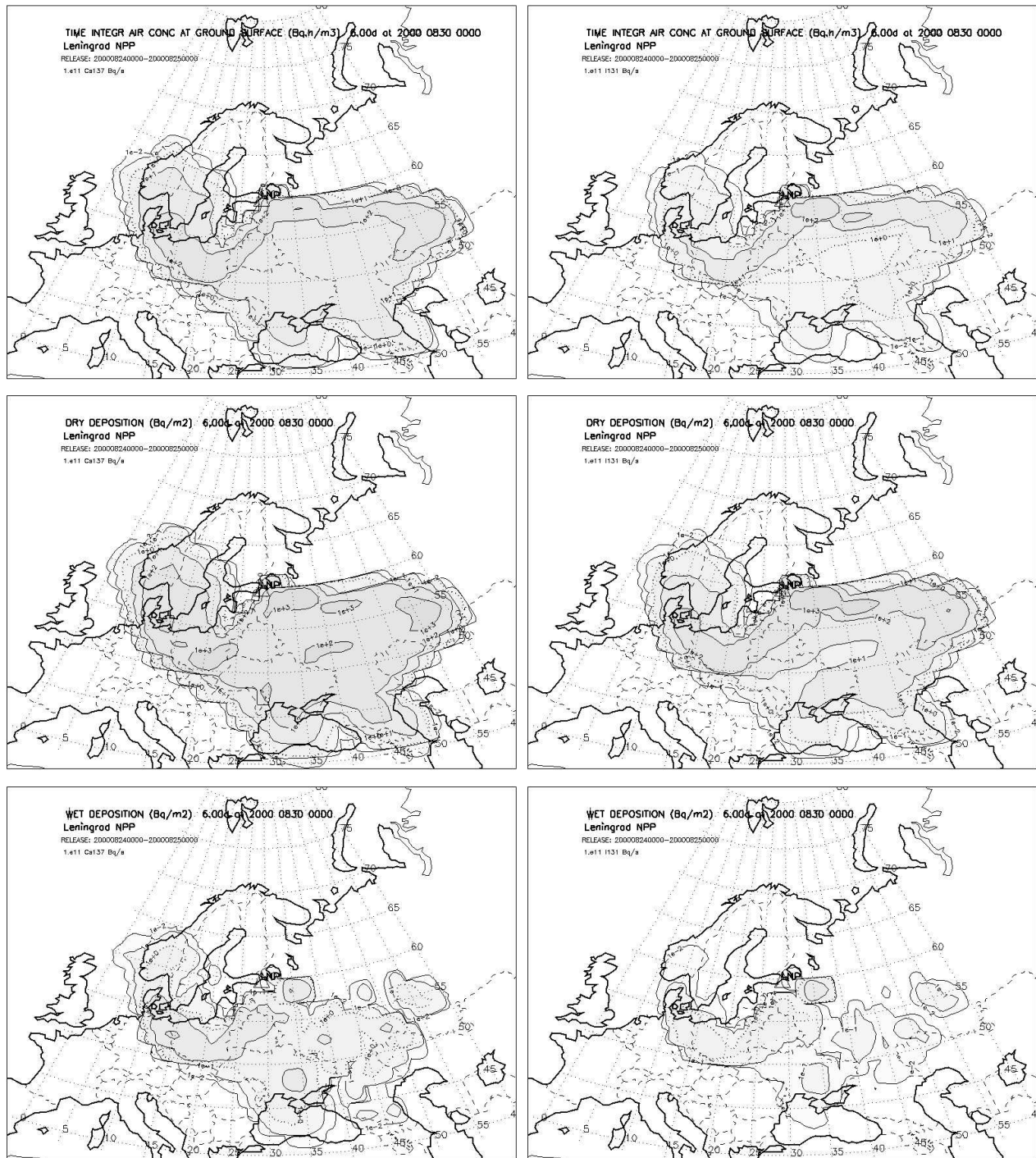
Fig. 8. Time integrated air concentration (top plate), dry deposition (middle plate), and wet deposition (bottom plate) fields of [137]Cs (left column) and [131]I (right column) on 6th day of atmospheric transport for the hypothetical release occurred (24–25 Aug. 2000, 00 UTC) at the Leningrad nuclear power plant.

T a b l e 4

Estimated time integrated air concentration, dry deposition, wet deposition, and relative contribution of wet deposition into total deposition for radionuclides at selected cites for the hypothetical release occurred (24–25 Aug. 2000, 00 UTC) at the Leningrad NPP (LNP)

City, Country	Distance to LNP, km	Time Integrated Air Concentration (TIAC), Bq·h/m^3			Dry Deposition (DD), Bq/m^2			Wet Deposition (WD), Bq/m^2			Wet Deposition/ Total Deposition, %		
		^{137}Cs	^{131}I	^{90}Sr	^{137}Cs	^{131}I	^{90}Sr	^{137}Cs	^{131}I	^{90}Sr	^{137}Cs	^{131}I	^{90}Sr
St.Petersburg, Russia	70	9.5E+0	8.5E+0	9.4E+0	5.1E+1	1.2E+2	6.8E+1	9.9E-2	5.7E-2	9.8E-2	0.2	<0.1	0.1
Tallinn, Estonia	245	1.9E-3	9.9E-6	1.1E-3	1.0E-2	2.1E-4	7.9E-3	0.0E+0	0.0E+0	0.0E+0	<0.1	<0.1	0.0
Helsinki, Finland	424	5.5E-1	3.0E-3	3.2E-1	3.0E+0	6.5E-2	2.3E+0	3.3E-3	1.8E-5	2.0E-3	0.1	<0.1	0.1
Riga, Latvia	435	5.0E-4	3.3E-6	3.0E-4	2.7E-3	6.9E-5	2.2E-3	7.6E-7	3.8E-9	4.5E-7	<0.1	<0.1	<0.1
Stockholm, Sweden	618	1.5E+1	1.8E-1	9.7E+0	8.2E+1	3.8E+0	7.0E+1	1.0E-4	2.9E-6	7.1E-5	<0.1	<0.1	<0.1
Vilnius, Lithuania	622	6.7E+1	1.3E+1	5.7E+1	3.6E+2	2.1E+2	4.1E+2	3.3E+1	5.1E+0	2.8E+1	8.4	2.4	6.5
Minsk, Belarus	673	1.2E+2	1.7E+1	9.9E+1	6.5E+2	2.8E+2	7.1E+2	3.9E+1	4.6E+0	3.3E+1	5.7	1.6	4.4
Moscow, Russia	686	3.5E+1	5.0E+0	2.8E+1	1.9E+2	7.9E+1	2.0E+2	1.4E-2	5.1E-4	1.0E-2	<0.1	<0.1	<0.1
Warszawa, Poland	983	1.4E+2	8.1E+0	1.0E+2	7.6E+2	1.4E+2	7.4E+2	8.6E+0	4.4E-1	6.5E+0	1.1	0.3	0.9
Oslo, Norway	1014	2.6E+1	5.2E-1	1.8E+1	1.4E+2	1.1E+1	1.3E+2	1.2E+0	2.1E-2	8.1E-1	0.8	0.2	0.6
Kiev, Ukraine	1057	3.1E+1	5.2E-1	2.1E+1	1.7E+2	1.0E+1	1.5E+2	4.3E+0	6.0E-2	2.8E+0	2.5	0.6	1.8
Copenhagen, Denmark	1077	1.6E+2	6.2E+0	1.2E+2	8.7E+2	1.2E+2	8.4E+2	9.8E+0	4.1E-1	7.2E+0	1.1	0.3	0.9
Berlin, Germany	1261	1.4E+2	8.6E+0	1.0E+2	7.3E+2	1.6E+2	7.4E+2	7.9E+1	4.6E+0	6.0E+1	9.7	2.8	7.5
Praha, Czech Republic	1426	3.9E+0	3.2E-1	3.0E+0	2.1E+1	5.6E+0	2.2E+1	1.5E+0	1.0E-1	1.2E+0	6.6	1.8	5.1
Bratislava, Slovakia	1515	4.8E-2	4.5E-3	3.8E-2	2.6E-1	7.9E-2	2.7E-1	6.7E-3	4.9E-4	5.3E-3	2.5	0.6	1.9
Budapest, Hungary	1522	2.6E-3	9.6E-6	1.5E-3	1.4E-2	2.1E-4	1.1E-2	1.6E-4	5.5E-7	8.8E-5	1.1	0.3	0.8
Vienna, Austria	1535	6.7E-3	5.9E-4	5.2E-3	3.6E-2	1.0E-2	3.8E-2	2.3E-3	1.6E-4	1.8E-3	6.0	1.6	4.6
Bucharest, Romania	1731	1.3E-1	1.2E-3	8.2E-2	7.0E-1	2.7E-2	5.9E-1	1.3E-3	1.2E-5	7.9E-4	0.2	<0.1	0.1

The TIAC fields for long-lived vs. short-lived (^{137}Cs vs. ^{131}I) radionuclides are shown in fig. 8, top. The shape and structure of TIAC are similar for long-lived nuclides: ^{137}Cs and ^{90}Sr (see [20]). The correlation coefficient between these two fields is high (0.98), because it is strongly dependent on the half-life of the nuclides ($9.50428 \cdot 10^8$ sec vs. $9.17640 \cdot 10^8$ sec for ^{137}Cs vs. ^{90}Sr, respectively) used in modelling of radioactive decay. Similar conclusion can be made about the DD fields. Since the LNP site is an inland site, the more continental type of climate than maritime is a peculiarity of this site compared, for example, with the BBP site. The strong dependence on the precipitation irregularity during atmospheric transport of the contaminated cloud is reflected in the wet deposition patterns. Hence, the structure of the WD field is more cellular compared with the TIAC and DD fields. The total area enclosed by the WD isolines is much smaller too (fig. 8, bottom).

Analyses of fields (shown in figs 8) allow identifying several features for this specific case. First, note that for the long-lived nuclides the shape and magnitude of isolines are similar for all fields, and it is due to very similar half-life times and reference dry deposition velocities for these radionuclides compared with ^{131}I. Second, for ^{131}I, the concentration decreases faster with distance from the site (similar with other calculated fields, although the rate of decrease is slower). Additionally, an area under a particular order of magnitude isoline could be calculated similarly to estimation of areas enclosed by isolines of the maximum reaching distance and maximum possible impact zone indicators (based on results of trajectory modelling, see [20]).

When several geographical locations/cities of interest are chosen than values of TIAC, DD, and WD can be calculated by interpolation from the original fields, as shown in tabl. 4. The highest ^{137}Cs TIAC (1.6e+2 Bq·h/m^3) was at Copenhagen, Denmark and the lowest — 5.0e–4 Bq·h/m^3 — at Riga, Latvia. Similarly, the highest ^{90}Sr TIAC — 1.2e+2 Bq·h/m^3 — at Copenhagen, Denmark, and the lowest — 3.0e–4 Bq·h/m^3 — at Riga, Latvia. The lowest ^{131}I TIAC (3.3e–6 Bq·h/m^3) was at Riga, Latvia; the highest (1.7e+1 Bq·h/m^3) was at Minsk, Belarus. A similar situation is found for the DD patterns vs. radionuclides, i. e. the highest and lowest magnitudes of DD for a particular radionuclide were observed at the same cities as for the concentrations. The lower TIACs and DDs for three cities — Budapest, Tallinn, and Riga — is a result of the later arrival of the contaminated cloud to these locations compared with other cities.

The highest ^{137}Cs WD (7.9e+1 Bq/m^2) was at Berlin, Germany and the lowest (7.6e–7 Bq/m^2) was at Riga, Latvia (at Tallinn, Estonia wet deposition did not even occur). Similarly, the highest ^{90}Sr WD (6.0e+1 Bq/m^2) — at Berlin, Germany and the lowest – 4.5e–7 Bq/m^2 — at Riga, Latvia. But, although the lowest ^{131}I WD (3.8e–9 Bq/m^2) was at Riga, Latvia, the highest — 5.1e+0 Bq/m^2 — at Vilnius, Lithuania. For this specific case, the contribution of wet deposition during atmospheric transport was ranging, in general, from less than 0.1 (shown in Tab. 4 as "<0.1" or negligible) to 9.7 % of the total deposition. Because of the natural (following the radioactive decay) faster decrease of ^{131}I concentration, especially during the first days of transport, the TIAC, DD, WD, and relative contribution of wet deposition were also several times smaller compared with other radionuclides. Hence, for this particular specific case the precipitation factor was not a significant contributor compared to average fields in § 2.2, and major role was played by the atmospheric transport, diffusion, and dry deposition.

3. Conclusion

The main aim of this study was to combine atmospheric transport and dispersion modelling and statistical analyses to assess consequences of an accidental release at the selected nuclear

risk sites (NRS) located in the Euro-Arctic region. The main purpose of this study was a probabilistic analysis of atmospheric transport and deposition patterns from these sites for GIS-based studies of vulnerability to radioactive deposition and risk assessment of impact.

The nuclear risk sites of concern selected in this study were 16 sites including nuclear power plants, nuclear submarine bases, nuclear processing plant, and former nuclear weapons testing site. The countries and geographical regions of interest are the Nordic countries, Baltic States, Eastern and Western European countries of the Northern Europe, Belarus, Ukraine, and the European territories of the Russian Federation.

In our study we tested the methodology developed within the "Arctic Risk" NARP Project [1, 2] and based on the long-term probabilistic dispersion modelling approach. The DERMA model was employed to simulate 5-day atmospheric transport, dispersion, and deposition of ^{137}Cs for a one-day release (at rate of 10^{11} Bq/s). As input data the DMI-HIRLAM and ECMWF meteorological gridded fields were used. A set of statistical methods for analysis of dispersion modelling results was employed. Additionally, the specific date (24th August of 2000) when atmospheric transport occurred towards the geographical regions of interest was studied on example of the Leningrad plant.

The results of the probabilistic analysis of dispersion modelling results for the risk sites were presented as a set of indicators of the risk sites impact on the geographical regions of interest. In this study, we calculated, constructed, and evaluated several indicators based on dispersion modelling results: time integrated air concentration (TIAC) at the ground surface, dry deposition (DD), and wet deposition (WD) patterns. To evaluate the temporal variability of these indicators, analyses were performed on an annual, seasonal, and monthly basis.

The general findings are the following. For the long-term simulation, the time integrated air concentration and dry deposition have higher values in vicinity of the sites, and decreasing by 1–2 orders of magnitude for approximately every 1000 km. Moreover, both types of fields have an elliptical form, which reflects the dominating airflow patterns from the sites throughout the year. For most of the sites these fields showed the prevailing atmospheric transport by westerly flows. Although wet deposition is also high near the sites, the WD field can have several local maxima remotely situated from the sites, this field is less smooth, and it has a cellular structure strongly depending on the irregularity of the rainfall patterns. Among 16 risk sites considered in this study several groups can be identified based on the temporal and spatial distribution of TIAC, DD, and WD fields. These groups consisted of the sites located in the maritime area, inland area, Arctic latitudes area, and intermediate area between the maritime and continental types of the climatic regimes.

Analysis of specific case showed several common peculiarities. First, shapes and magnitude of isolines are almost similar for both ^{137}Cs and ^{90}Sr TIAC and DD fields, and both fields are well correlated. Second, ^{131}I TIAC decreases faster with distance from the site compared with ^{137}Cs and ^{90}Sr due to radioactive decay and greater possibility to serve as condensation nuclei. Third, the WD fields showed a similar structural irregularity (as seasonal and monthly variability) compared with the TIAC and DD fields.

Further, it is planned to use such results in different dose calculation models as well as the GIS-based risk and vulnerability analysis for population and environment, first of all, of the Nordic countries. We suggest that the methodology developed within the "Arctic Risk" NARP Project [1] and tested in this study can be successfully applied for other sites of concern such as chemical, biological, and natural hazards, for assessments of the long-term impacts from existing emission/release sources of different kinds of pollutants as well as for environmental problems of wider spectra.

4. Acknowledgments

References

[1] AR-NARP (2001–2003) Atmospheric Transport Pathways, Vulnerability and Possible Accidental Consequences from the Nuclear Risk Sites in the European Arctic (*Arctic Risk*) of the NARP: Nordic Arctic Research Programme.
DMI project web site: `http://glwww.dmi.dk/f+u/luft/eng/arctic-risk/main.html`.

[2] BAKLANOV A., MAHURA A., SØRENSEN J.H. ET AL. (2002B) Methodology for Risk Analysis based on Atmospheric Dispersion Modelling from Nuclear Risk Sites. Danish Meteorological Institute, Sci. Report, 02-16. 54 p.

[3] BAKLANOV A. Methodologies for multidisciplinary nuclear risk and vulnerability assessments in the Arctic and Sub-Arctic. NATO Science Series, Kluwer Academic Publ., 2002.

[4] BAKLANOV A., BERGMAN R., SEGERSTÅHL B. Radioactive Sources in the Kola Region: Actual and Potential Radiological Consequences for Man. Report, International Institute for Applied Systems Analysis. Laxenburg, Austria, IIASA, Radiation Safety of the Biosphere, 1996. 255 p.

[5] MOBERG L. (ED.) The Chernobyl Fallout in Sweden. Results From a Research Programme on Environmental Radiology. The Swedish Radiation Protection Institute, Stockholm, Sweden, 1991.

[6] BERGMAN R., THANING L., BAKLANOV A. Site-sensitive Hazards of Potential Airborne Radioactive Release From Sources on the Kola Peninsula. FOA report: FOA-RЧ00717-861–SE, February 1998. 14 p.

[7] DAHLGAARD H. (ED.) Nordic Radioecology: The transfer of radionuclides through Nordic ecosystems to man. Amsterdam, Elsevier Science B. V. Studies in Environmental Science. 1994. Vol 62.

[8] BERGMAN R., ULVSAND T. Intervention in regular practice to bring down external exposure to agricultural personnel or activity transfer over certain boreal food-chains. FOA Report, National Defence Research Establishment, Dept of NBC Defence, S-90182 Umeå, Sweden. 1994.

[9] AMOSOV P.V., BAKLANOV A.A., MAZUKHINA S.I. Estimation of potential risk for the population from the hypothetical accident at the Kola nuclear power plant // The 2nd Intern. Conf. on Environmental Radioactivity in the Arctic. Oslo, Aug. 21–25, 1995. P. 365–368.

[10] RANTALAINEN L. Source terms of the Kola nuclear power plant and risk of severe environmental contamination // The 2nd Intern. Conf. on Environmental Radioactivity in the Arctic. Oslo, Aug. 21–25, 1995.

[11] SALTBONES J., FOSS A., BARTNICKI J. Threat to Norway from potential accidents at the Kola nuclear power plant. Climatological trajectory analysis and episode studies // Atmospheric Environment. 2000. Vol. 34(3). P. 407–418.

[12] BAKLANOV A., MAHURA A., JAFFE D. ET AL. Atmospheric transport patterns and possible consequences for the European North after a nuclear accident // J. of Environmental Radioactivity. 2002. Vol. 60. P. 23–48.

[13] MAHURA A.G., JAFFE D., ANDRES R., MERRILL J. Atmospheric transport pathways from the Bilibino nuclear power plant to Alaska // Atmospheric Environment. 1999. Vol. 33/30. P. 5115–5122.

[14] SLAPER H., EGGINK G.J., BLAAUBOER R.O. Risk assessment method for accidental releases from nuclear power plants in Europe. Report of the National Institute of Public Health and the Environment. Bilthoven, Netherlands, 1994.

[15] NATO (1998): Cross-Border Environmental Problems Emanating from Defence-Related Installations and Activities. NATO/CCMS Pilot Study, Phase II: 1995–1998, Final Report. Vol 4. March 1998. P. I-81–84.

[16] SINYAK Y. Nuclear Energy in Eastern Europe and the Former Soviet Union: How Safe and How Much? International Institute for Applied Systems Analysis (IIASA) Sci. Report, Sum. 1995.

[17] ANDREEV I., HITTENBERGER M., HOFER P. ET AL. Risks due to severe accidents of nuclear power plants in Europe — the methodology of riskmap // J. Hazardous Materials. 1998. Vol. 61. P. 257–262.

[18] ANDREEV I., GAZSO A., GOHLA H. ET AL. Risks due to severe accidents of nuclear power plants in Europe — the methodology of RISKMAP Ц Possible extensions // ESEE 2000: 3rd Intern. Conf. of the European Society for Ecological Economics. 2000.

[19] BAKLANOV A., MAHURA A. Atmospheric Transport Pathways, Vulnerability and Possible Accidental Consequences from the Nuclear Risk Sites: Methodology for Probabilistic Atmospheric Studies. DMI Sci. Report N 01-9. 2001.

[20] MAHURA A., BAKLANOV A., SØRENSEN J.H. Long-Term Atmospheric Transport and Deposition Patterns from Nuclear Risk Sites in Euro-Arctic Region. Danish Meteorological Institute, Sci. Report, N 02-15, 2002.

[21] BAKLANOV A.A., MAHURA A.G., MOROZOV S.V. The simulation of radioactive pollution of the environment after an hypothetical accident at the Kola Nuclear Power Plant // J. Environmental Radioactivity. 1994. Vol. 25. P. 65–84.

[22] THANING L., BAKLANOV A. Simulation of atmospheric transport and deposition on the local/meso- and regional scales after hypothetical accidents at Kola Nuclear Power Plant // Sci. Tot. Environmental. 1997. Vol. 202. P. 199–210.

[23] BAKLANOV A. Modelling of episodes of atmospheric transport and deposition: Hypothetical nuclear accidents in North-West Russia // Nuclear Risks, Environmental and Development Co-operation in the North of Europe. CERUM, University of Umea, Sweden, 2000. P. 57–72.

[24] BAKLANOV A., BERGMAN R., LUNDSTRŐM C., THANING L. Modelling of Episodes of Atmospheric Transport and Deposition From Hypothetical Nuclear Accidents on the Kola Peninsula. CERUM Northern Studies Working Paper N 23. Umeåuniversity, Sweden, 2001.

[25] BAKLANOV A., SØRENSEN J.H. Parameterisation of radionuclide deposition in atmospheric dispersion models // Phys. Chem. Earth. (B). 2001. Vol. 26. P. 787–799.

[26] BAKLANOV A.A., MAHURA A.G. Assessment of possible airborne impact from risk sites: methodology for probabilistic atmospheric studies // Atmospheric Chemistry and Physics. 2004. Vol. 4(2). P. 485–495.

[27] RIGINA O., BAKLANOV A. Regional radiation risk and vulnerability assessment by integration of mathematical modelling and GIS-analysis // Environment International. 2002. Vol. 27. P. 527–540.

[28] BAKLANOV A., MAHURA A., SØRENSEN J.H. Methodology for Prediction and Estimation of Consequences of Possible Atmospheric Releases of Hazardous Matter: "Kursk" Submarine Study. Atmospheric Chemistry and Physics. 2003. Vol. 3. P. 1–42.